The Refractive Index Spectra within Clouds from Forward-Scatter Radar Observations

EARL E. GOSSARD AND RICHARD G. STRAUCH

NOAA/ERL/Wave Propagation Laboratory, Boulder, CO 80303

(Manuscript received 28 July 1980, in final form 8 November 1980)

ABSTRACT

When long-wavelength radars are used to observe the atmosphere, there are occasions when radar return from a volume of cloud is unexpectedly large relative to that predicted by the classical incoherent scatter from individual cloud droplets. The assumption of incoherence predicts the scattered power to be proportional to the inverse fourth power of the wavelength. The observed weaker wavelength dependence could result from Bragg-coherent scatter from the ensemble of droplets or it could result from an enhancement by the cloud of inhomogeneities in the dielectric constant of the gaseous medium within the cloud. Both mechanisms are discussed and compared with data acquired in a forward-scatter mode by two 3 cm wavelength radars of NOAA's Wave Propagation Laboratory. Observed differences between the in-cloud and out-of-cloud refractive index spectra are discussed and conclusions are suggested.

1. Introduction

If incoherent scatter from an ensemble of individual cloud droplets is the only process causing radar return from a volume of cloud, the scattered power should be proportional to the inverse fourth power of the wavelength. However, the reflectivity of clouds observed by long-wavelength radars is sometimes unexpectedly high for the drop-size distribution measured or presumed to exist in the cloud type being observed. [For an example in which radar data were compared with particle size spectrometer data measured with an in-cloud aircraft see Gossard (1979).] Such observations suggest a weaker wavelength dependence than λ^{-4}. Two possible explanations for reflectivities higher than predicted by the inverse fourth power are 1) a Bragg component in the reflectivity of the cloud droplet ensemble from spatial variations in droplet concentration organized on a scale of $\lambda/2$, and 2) a cloud-enhancement of the Bragg reflection from the intracloud gas; i.e., cloud enhancement of the power density in the gaseous dielectric spectrum responsible for the usual clear-air scatter that would lead to a wavelength dependence of $\sim\lambda^{-1/3}$. Any important Bragg contribution from either mechanism would require that the usual interpretation of the reflectivity in terms of drop size and number density would have to be abandoned or substantially modified because of the very different wavelength/drop-size dependencies of the two types of scatter. The Bragg contribution is particularly important for long-wavelength radars such as those used in present and proposed wind profiling systems.

Gossard (1979) has compared Bragg-coherent scatter from the droplets themselves, when their concentration is spatially organized (perhaps by turbulence), with the Bragg coherent scatter to be expected from inhomogeneities in dielectric constant of the gaseous medium in the cloud. He points out that the gaseous refractive index variance is given by

$$\overline{\delta n^2} \times 10^{12} \simeq 58.5\overline{\delta Q_v^2} + 2.04\overline{\delta T^2} - 21.9\overline{\delta T \delta Q_v}, \quad (1)$$

where δT is the temperature perturbation and δQ_v the perturbation of the mixing ratio of water vapor. The constants depend on mean temperature, humidity and pressure p, and in (1) it is assumed that $T \approx 280$ K, $p \approx 1000$ mb and $Q_v \approx 8$ g kg^{-1}.

On the other hand, Gossard finds the variance of the equivalent refractive index of the liquid water droplet medium to be given by

$$\delta n_e^2 \times 10^{12} = (9/4)|K|^2(\rho_a/\rho_{L,I})^2\overline{\delta Q_{L,I}^2} \approx \begin{cases} 2.09\overline{\delta Q_L^2} & \text{for water} \\ 0.52\overline{\delta Q_I^2} & \text{for ice,} \end{cases} \quad (2)$$

where $|K|^2 \approx 0.93$ for water, $|K|^2 \approx 0.21$ for ice, ρ_a is the density of air, $\rho_{L,I}$ is the density of the water or ice spheres, and $\overline{\delta Q_{L,I}^2}$ is the variance of the mixing ratio of liquid water or ice (i.e., mass of liquid water or ice per mass of dry air). The density of water has been assumed to be 10^6 g m^{-3} and that of ice 0.91×10^6 g m^{-3}.

The factor 58.5 multiplying the water vapor variance term in Eq. (1) is large compared with the corresponding factor multiplying temperature vari-

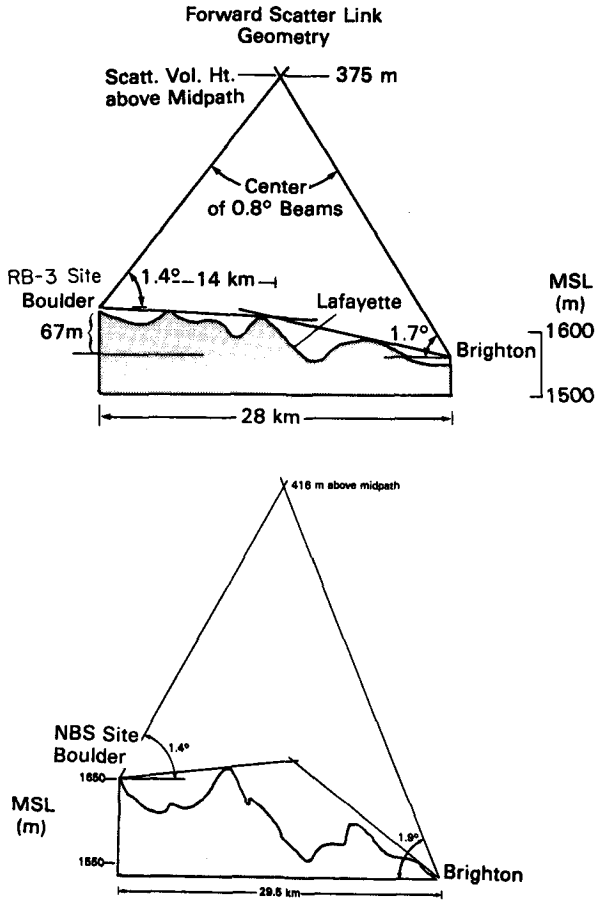

FIG. 1. The terrain profiles relative to the forward scatter geometry for grazing elevation angles. The first principal null in the antenna pattern was placed on the terrain horizon at the Brighton end of the path. The null is about 1.4° off the main lobe as seen in Fig. 2.

ance so gas density variance is relatively unimportant. That is a result of the bipolar character of the water molecule and its resulting dipole moment. If the vapor mixing-ratio variance is the same as the variance of the liquid and/or ice mixing ratios, there is a strong bias toward scatter from the gas, compared with scatter from the liquid water or ice droplets, amounting to a factor of almost 30 for water and an additional factor of about 4 for ice. Thus, the expected relative magnitudes of liquid, ice and vapor variances in clouds are decisive in determining the important coherent scattering mechanism. For steady state in a nonprecipitating cloud at saturation, a given change in mixing ratio of liquid water produces a corresponding change of opposite sign in water vapor mixing ratio, so it is reasonable to assume the variances are of comparable magnitude. Thus this logic seems capable of almost ruling out Bragg scatter from cloud droplets as an important mechanism compared with gaseous scatter. However, it is possible that there is some mechanism by which the cloud microphysics thermodynamically enhances the refractive index variance of some clouds by increasing the dielectric Bragg backscatter from the gaseous medium of the cloud. For example, it was pointed out by Gossard (1979) that the cloud model of Clark and Hall (1979) predicts thermodynamic enhancement of $\overline{\delta Q_v^2}$, from supersaturation resulting from the relaxation time of the evaporation/condensation process, that is comparable to that generated by the turbulence cascade. Clearly, it is important to carry out decisive experiments to determine whether there really is substantial enhancement of cloud reflectivity contributed by a Bragg (coherent) component.

This paper describes results obtained by an observational technique that is capable of separating Bragg-coherent scatter from the incoherent scatter usually presumed to dominate cloud or precipitation reflectivity. It reveals the spatial spectral form of refractive index perturbations within the cloud for comparison with spectra in the clear air. It uses the dependence of signal strength on scattering angle to separate incoherent scatter from Bragg scatter by recognizing that Bragg scatter is strongly angle dependent, while incoherent scatter has no dependence on the horizontal component of the scattering angle if the radar polarization is vertical. It clearly reveals the wavelength where transition from incoherent scatter dominance to Bragg scatter dominance occurs.

2. The observational program

Two Doppler radars of 3.2 cm wavelength were placed at opposite ends of a path between Boulder and Brighton near Denver, Colorado. The topography and geometry were carefully chosen such that the terrain prevented the direct, line-of-sight signal of the transmitting radar from entering the receiver of the other even when both antennas were pointing toward each other along the great circle path (hereafter called the baseline) joining the radars. The terrain profiles are shown in Fig. 1.

During the spring of 1979 the receiving radar at Boulder was operated at the site designated RB-3. The Boulder radar was then moved to the site labeled NBS to avoid obstruction by the new foliage on trees near the radar path, but the presence of flying insects prevented data collection during the summer. Data collection, especially in the clear air, was resumed in the fall. The character of the horizon was considered to be very important to avoid diffraction and scattering from objects such as powerlines, metal buildings, silos and metal towers; in fact, two sites were tried and rejected before the final sites were chosen. The horizons were examined optically by theodolite and by on-site inspection, and the radar return was carefully

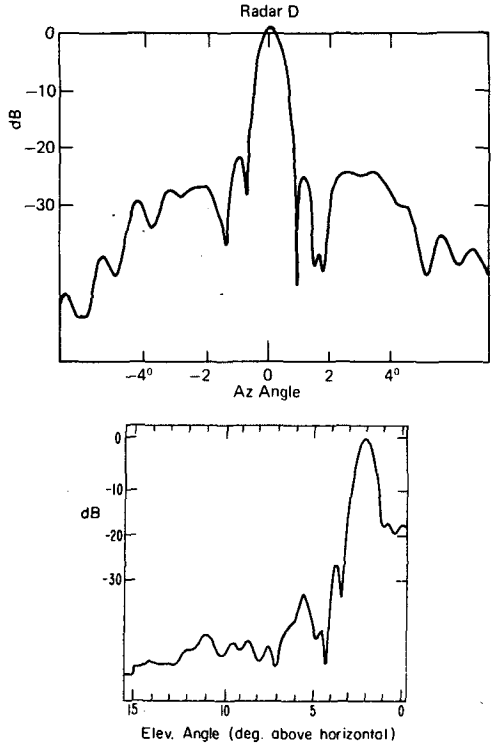

FIG. 2. Antenna patterns for the 3.2 cm wavelength Doppler radars used in the experiment.

examined as the beams were swung horizontally along the horizon in both forward and backscatter. To minimize horizon effects the lowest elevation angle was chosen so that the first principal null in the antenna patterns was placed essentially on the terrain horizon.

In Fig. 1 the center of the beam of the Boulder radar is shown at an elevation angle of 1.4°, which was the minimum used. Fig. 2 shows that the elevation angle between the main lobe and the first principal null in the antenna pattern (at 3.7°) is also 1.4°. At the RB-3 site the angle between the beam axis and the horizon is 1.5° and at the NBS site the angle is 1.3°. At the Brighton end, the angle between the beam axis and the horizon is 1.4° in both cases. Thus at the minimum elevation angle used, the local horizon was essentially in the first principal null. As the beam was swung horizontally, the angles to the local horizons changed slightly, but the terrain about the path was very flat.

Fig. 2 shows the gain of the main lobe above the first side lobe in the horizontal antenna pattern to be ~27 dB for both transmission and reception or 54 dB total; therefore, essentially all of the signal can be attributed to the common volume of the main beams of the antenna as the beams are swung horizontally. The antenna beamwidths (between 3 dB points) are 0.8°; thus they can be considered to be a narrow-beam system in the sense that the effective scattering volume is limited by the common volume of intersection of the transmitting and receiving antennas rather than by the scattering properties of the atmosphere (Booker and DeBettencourt, 1955).

The geometry of the forward scatter path is shown in Fig. 3. The distances from the transmitter to the scatterer and from the scatterer to the receiver are $\mathbf{r}_0$ and $\mathbf{r}_s$, respectively. Simple trigonometry shows that the vector difference between $\mathbf{k}_0$ and $\mathbf{k}_s$ has a magnitude of $|\mathbf{k}|2\sin(\theta/2)$. It is called the Bragg wavenumber, here designated κ.

The experimental procedure was to vary the scattering angle θ by changing antenna azimuths to swing both beams together off midpath. Thus, the altitude of the scattering volume remains the same, and a measure of power versus the Bragg wavenumber is obtained. This relationship unambiguously determines the spectrum $\phi(\kappa)$ of the spatial distribution of the scattering ensemble as will be shown in the following section. If the scattering is coherent in the Bragg sense, the scattering should be strongly in the forward direction from transmitter to receiver. If it is fundamentally incoherent, it should be independent of scattering angle except for the geometrical effect on the size of the scattering volume. For our geometry the minimum scattering angle at one site, designated RB-3, was 3.07° corresponding to an on-baseline elevation angle of 1.4° at the Boulder site and 1.7° at the site at Brighton. At the site designated NBS the minimum scattering angle was 3.66° and the elevation angle at Brighton was 1.9°. As the beams were swung horizontally, power versus azimuth patterns were obtained like those shown in Fig. 4. The orientation of the baseline from Boulder was 91.4° east of true north at the RB-3 site and 87.1° at the NBS site. Usually, several elevation angles were used between 1.4 and 2.0° at the Boulder site. Occasional recordings of signal versus elevation angle on the base-

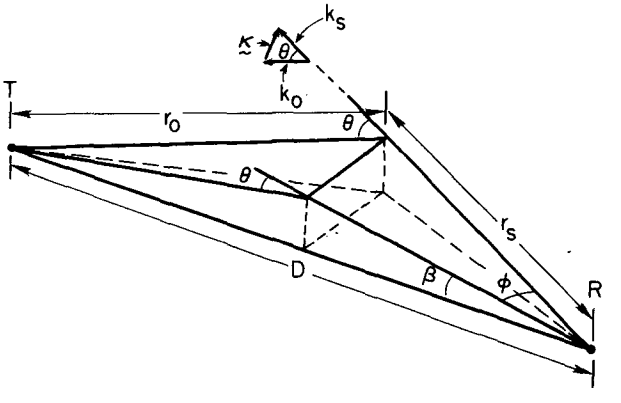

FIG. 3. Schematic picture of the beam-swinging experiment.

line (vertical beam swinging) were made to obtain height profiles of C_n^2 and power spectra.

When cloud or precipitation provided measurable backscatter, the Brighton radar recorded backscatter continually along the radio path, while the Boulder radar alternated forward scatter reception with backscatter measurements. The backscatter was assumed to be purely incoherent scatter at the 3.2 cm wavelength of these radars and was used to remove the incoherent component from the total forward scatter so that the Bragg component could be extracted. (See in Fig. 4 the break in the received power function near Az = 4° where the Bragg component falls to levels comparable to the incoherent "floor.") The minimum detectable signal for the radar is −103 dBm.

Experiments were carried out in both clear-air and cloud conditions for comparison. As seen in Fig. 4, the forward scatter was always dominated by angle-dependent Bragg coherent scatter out to about 3–4 azimuthal degrees from the baseline. When there was significant cloud or precipitation scatter, the return at greater angles was essentially independent of azimuth, providing a clearly identifiable transition from the Bragg-coherent regime to the incoherent regime.

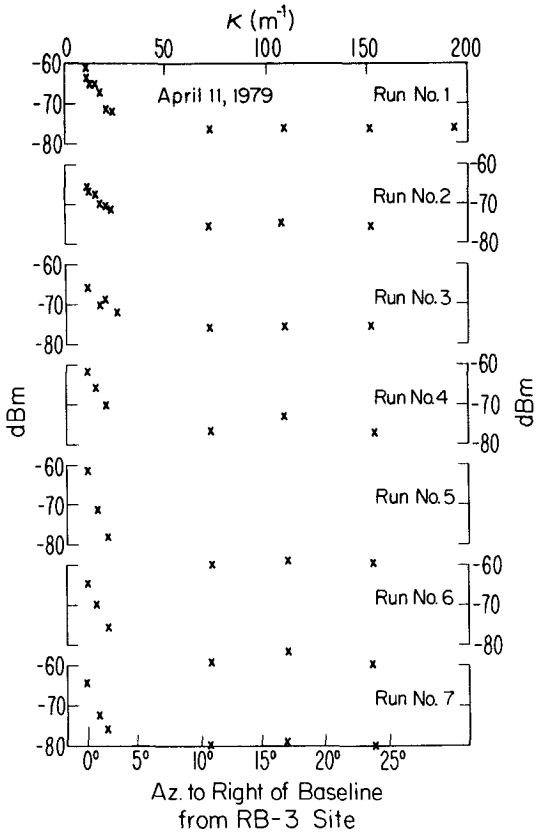

FIG. 4. Received power versus azimuth angle from baseline (bottom scale) or versus Bragg wavenumber (top scale) on 11 April 1979.

3. Formulation of the analysis

The scattered power at distance r_s from a volume of scatterers V is

$$P_s = \frac{P_0 V}{4\pi r_s^2}\eta, \tag{3}$$

where P_0 is the power density incident on the volume and η the reflectivity. If the scattered power is coherent in the Bragg sense and if inhomogeneities in the scattering medium are isotropic

$$\eta = 8\pi^2 k^4(\sin^2\chi)\phi(\boldsymbol{\kappa}) \equiv 2\pi k^4(\sin^2\chi)\phi(\kappa)/\kappa^2, \tag{4}$$

where the three-dimensional power spectrum in vector $\boldsymbol{\kappa}$ is $\phi(\boldsymbol{\kappa})$. It is equal to $\phi(\kappa)/4\pi\kappa^2$ if the spectrum of refractive index is isotropic where $\phi(\kappa)$ is the "power" spectral density of the scattering inhomogeneities[1] in scalar κ. Here $\kappa = 2k\sin\theta/2$ is the Bragg wavenumber, $k = 2\pi/\lambda$, λ is radio wavelength, θ the scattering angle defined as the angle between the incident and scattering directions, and χ the angle between the electric vector and the scattering direction.

On the other hand, suppose the scattering is completely incoherent in the sense that the total scattered power is just the sum of the powers scattered by all of the individual scatterers. If the scatterers are spheres whose size is small compared with the radar wavelength, they radiate a wave like that of a Hertzian dipole. Thus the field is radially symmetrical about the axis of the incident electric vector, and the scattered field is the same as in backscatter for any azimuthal direction. For scattering in a direction other than 90° from the electric vector (say, χ), a geometrical factor ($\sin^2\chi$) must be included as in Eq. (4). The backscattered reflectivity is given in many texts (e.g., Battan, 1973) so, with the $\sin^2\chi$ correction for an arbitrary scattering direction, the reflectivity from an ensemble of small drops is

$$\eta = (\pi/16)k^4|K|^2(\sin^2\chi)Z, \tag{5}$$

where $Z = \sum N_i D_i^6$ is a "reflectivity factor" and represents a sum over unit volume of the number of scatterers N_i of diameter D_i. The quantity

$$|K|^2 = \left|\frac{(\epsilon/\epsilon_0) - 1}{(\epsilon/\epsilon_0) + 2}\right|^2 \approx 0.93$$

for liquid water drops at a wavelength of 3.2 cm

[1] At this point we do not specify the source or nature of the inhomogeneities. They may result from dielectric fluctuations in the gaseous atmosphere, or they may result from liquid (or ice) droplets whose spatial concentration is correlated over separations long compared with half the radar wavelength.

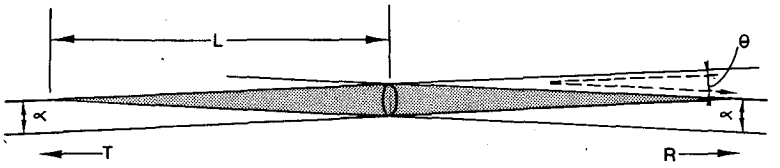

FIG. 5. Schematic picture of forward-scattering volume.

(e.g., see Battan, 1973); ϵ is the dielectric constant of the scatterer and ϵ_0 the dielectric constant of the propagation medium.

Noting that $P_0 = P_T G_T/4\pi r_0^2$ and $P_R = P_s A_e = P_s G_R \lambda^2/4\pi$, Eq. (3) shows that the received power is given by

$$P_R = \frac{P_T G^2 \lambda^2}{(4\pi)^3 r_s^2 r_0^2} V\eta, \tag{6}$$

where $G = G_R = G_T$, P_T is transmitted power and r_0 is distance from the transmitter to the scatterer. Near midpath $r_s \approx r_0 \approx D/2$. In backscatter, the volume intercepted by the radar beam is just $V = \pi D^2 \alpha^2 \Delta/16$ (for a "top-hat" beam) where Δ is the spatial resolution (half the pulse length) and D is the two-way path length; thus using Eq. (5) for incoherent backscatter,

$$V\eta = (\pi/4)^4 |K|^2 \alpha^2 k^4 D^2 Z\Delta/16, \tag{7}$$

where α is the antenna beamwidth. In this paper we will be mainly concerned with the scatter in the forward direction from narrow (0.8°) symmetrical beams which are the same at both the receiver and the transmitter.

In forward scatter the volume can therefore be represented schematically as shown in Fig. 5. The total volume is fairly well represented by two more-or-less conical volumes whose bases are circular sections of diameter $\alpha D/(2\cos^2\theta/2)$ and whose length $L \approx \alpha D/[4 \sin(\theta/2) \cos(\theta/2)]$, so

$$V \approx 2(1/3)\pi\alpha^3 D^3/[64\text{-}\cos^5(\theta/2) \sin(\theta/2)], \tag{8a}$$

or

$$V \approx (2\pi/3)\alpha^3 D^3/32\theta = \alpha^3 D^3/15.3\theta, \quad \text{for } \theta \ll 1. \tag{8b}$$

For a volume symmetrical about midpath we see from Eqs. (4) and (6) that

$$P_R = \{P_T G^2 \lambda^2/(4\pi)^2 D^2\} 32\pi k^4 (\sin^2\chi) V\phi(\kappa)/D^2$$
$$= P_{FS} V(4/\pi)\eta/D^2 \tag{9}$$

for Bragg scatter, where the factor in braces is the "free-space" power P_{FS} at distance D.

For incoherent forward scatter Eqs. (6) and (5) give

$$P_R = P_{FS} V |K|^2 k^4 (\sin^2\chi) Z/4D^2. \tag{10}$$

For Bragg scatter from homogeneous, isotropic turbulence, it is convenient to express the scatter in terms of the structure constant of refractive index C_n^2. The one-dimensional spectrum along a line in space $\phi_1(\kappa)$ is related to C_n^2 such that

$$\phi_1(\kappa) \approx \tfrac{1}{4} C_n^2 \kappa^{-m}, \tag{11}$$

where $m = -5/3$ for a Kolmogoroff spectrum (Tatarskii, 1961; Ottersten, 1969). However, the power spectral density is related to the one dimensional spectrum along a line such that

$$\phi(\kappa) = -\kappa \frac{\partial\phi_1}{\partial\kappa} \quad \text{(Kovasnay } et\ al.\text{, 1949; Bolgiano, 1958).} \tag{12}$$

Thus

$$\phi(\kappa) = (1/4) m C_n^2 \kappa^{-m} \tag{13}$$

and

$$\phi(\kappa) = (m/16\pi) C_n^2 \kappa^{-(2+m)}, \tag{14}$$

so Eq. (9) becomes [using Eqs. (4) and (14)]

$$P_R = P_{FS}(V/D^2) k^4 (\sin^2\chi) 2m C_n^2 \kappa^{-(2+m)}. \tag{15}$$

In our experiment

$$P_T = 20 \text{ kW}$$
$$\lambda = 0.032 \text{ m}$$
$$\alpha = 0.8°$$
$$G = (\pi/\alpha)^2 = 47 \text{ dB}$$
$$D = 28 \text{ km}; 29 \text{ km}$$
$$\sin\chi \approx 1.0.$$

Comparing values of backscatter reflectivity at midpath, a difference in the transmitted power of the two radars was detectable. Therefore, 2 dB was added to the received backscatter power at the Boulder site. The values of Z from the two radars were then calculated and averaged. With this correction the absolute accuracy of the measured power is ±1 dB. The relative accuracy as the beam is swung azimuthally away from the baseline, of course, is much better.

4. Observational results

The observed spectra for various events are shown in Figs. 6–13. The data in Figs. 6–10 were obtained with the receiver at the Boulder RB-3 site and the data of Figs. 11–13 were obtained at the NBS site. The beams were swung both right and left of the great circle path (baseline) joining the radars and the results were essentially the same.

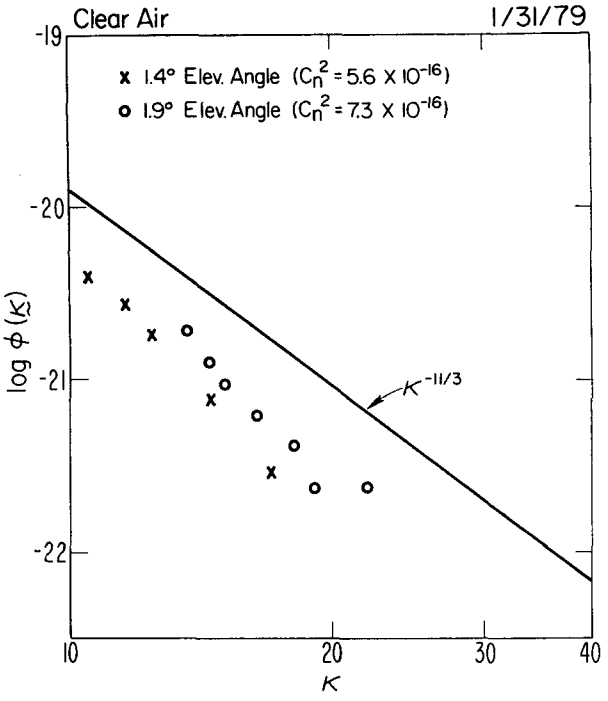

FIG. 6. Scatterer spectra calculated from forward-scatter signals measured close to baseline during azimuthal beamswinging. Brighton to RB-3 path. Weather clear. Excellent visibility. Lenticular clouds over mountains west of path. Solid line shows −11/3 slope with arbitrary ordinate.

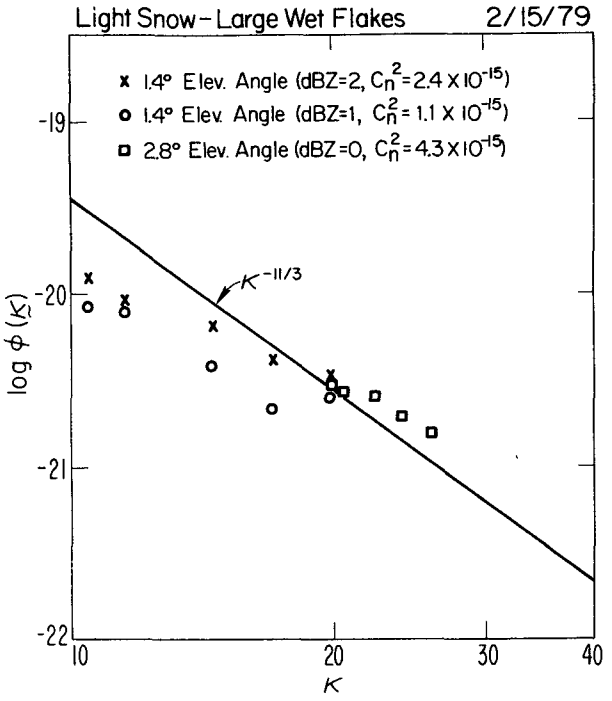

FIG. 7. Scatterer spectra on the Brighton to RB-3 path. Fog/clouds down to 750 m AGL. Snow began at 0915 MST when experiment began. Large, fairly dry flakes. Fine crystalline structure.

For those runs recorded and processed, the beams were swung in the direction considered to be best for the experiment. At the RB-3 site the beams were swung south of the baseline because there was less shrubbery and fewer trees to provide possible degradation of the radar beam. At the NBS site the beams were also swung toward the south because a power plant stack and a power line might have caused some deleterious effects if they had been swung north. However, such effects were sought and not found when the beams were swung toward the north. If the spectra had obeyed the Kolmogorov law for the inertial subrange, the slope of the $\log\phi(\kappa)$ vs $\log\kappa$ relation should be $-11/3$. The $-11/3$ slope is indicated by the solid curve on each figure. For the clear-air cases the average slope is -3.7 which is very close to the theoretical, but there is considerable deviation on individual days.

The average spectrum slope for the days having clouds and precipitation is -2.9 which is substantially less than the theoretical. However, again the scatter on individual days was large for both m and the apparent C_n^2. Regression lines on log-log scales were fitted to the experimentally observed spectra, and m was calculated for each spectrum. The values were then averaged for all spectra obtained during each event. The results are presented in

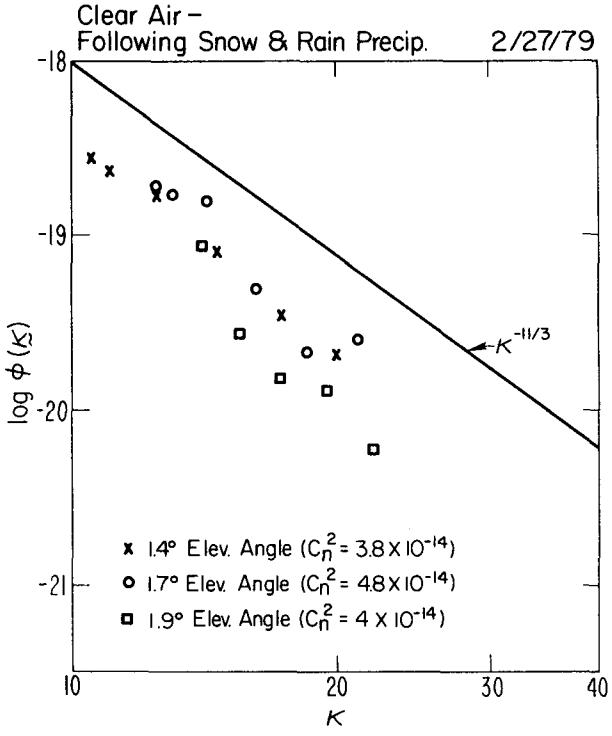

FIG. 8. Scatterer spectra on the Brighton to RB-3 path. Clouds/precipitation stopped about 1200 MST. Fractocumulus and spotty echoes when radar observations began at 1445 MST.

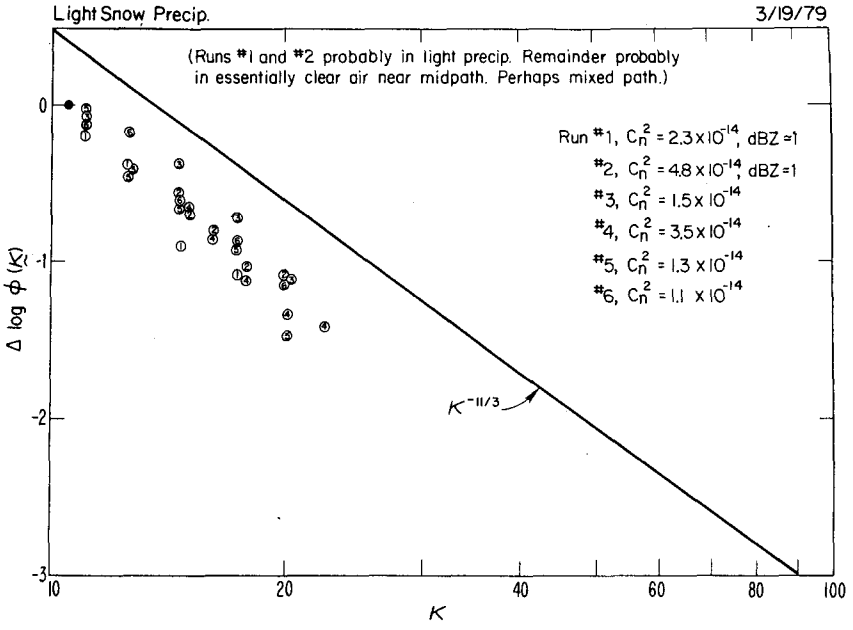

FIG. 9. Scatterer spectra on the Brighton to RB-3 path. Water and graupel mixed. Continuous small graupel by 1500 when observation began. The ordinate $\Delta \ln\phi(\kappa)$ is the departure from the on-baseline value of $\ln\phi(\kappa)$.

Table 1. If the observed m is assumed to apply over the whole spectral range instead of the 20–50 cm scales where it was measured, C_n^2 might be calculated from Eq. (15) using the observed value of m and the received power P_R. However, C_n^2 calculated in this manner is dominated by m, and we have considered it more meaningful to calculate C_n^2 assuming $m = 5/3$, and average it over the points

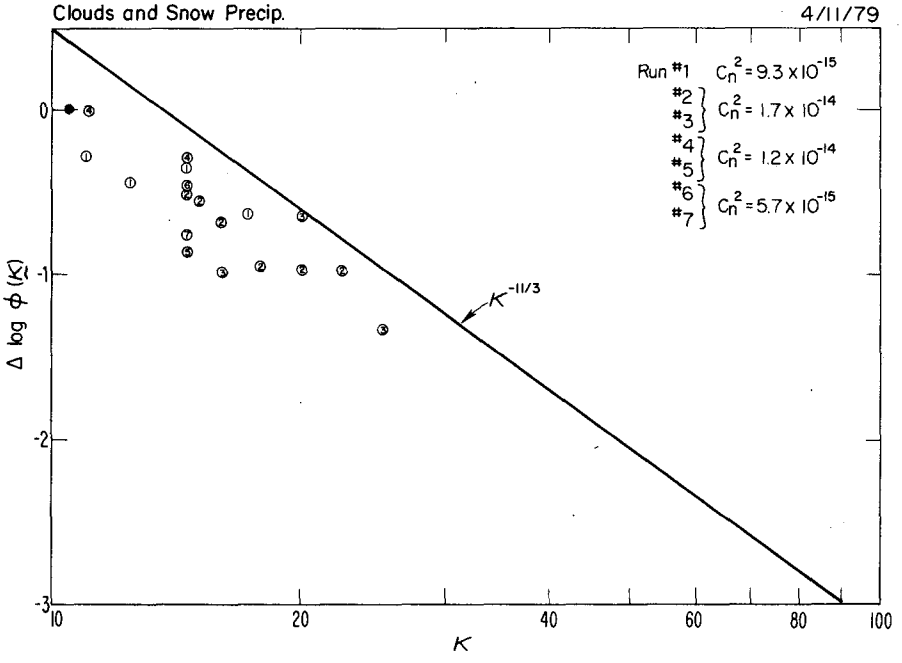

FIG. 10. Scatterer spectra on the Brighton to RB-3 path. Geometry as in Fig. 1 except runs 2 and 3 were done at an elevation angle of 2°. The ordinate $\Delta \ln\phi(\kappa)$ is the departure from the on-axis value of $\ln\phi(\kappa)$. Clouds and snow precipitation diminishing during experiment. Time history of fluctuations in dBZ is shown in Fig. 14.

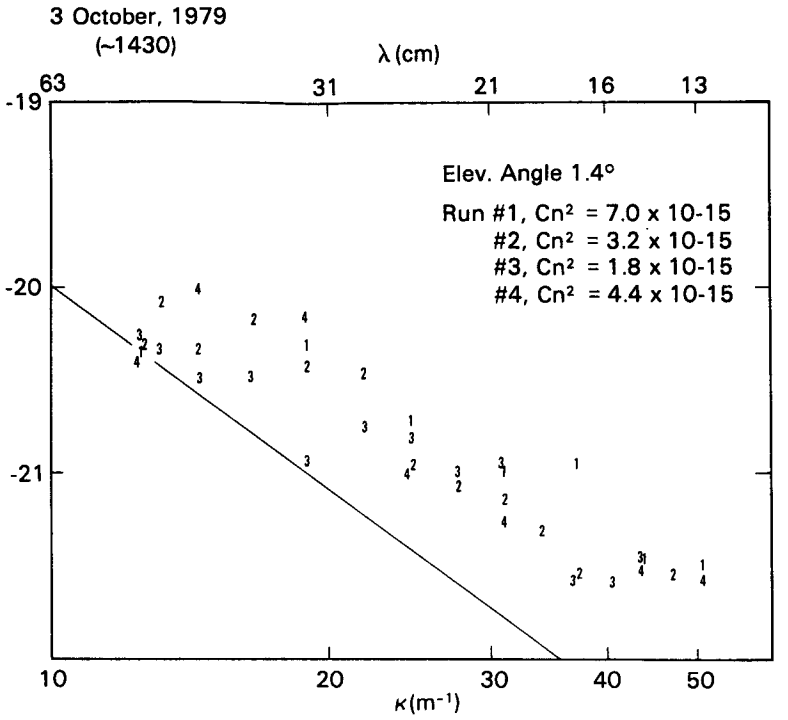

FIG. 11. Scatterer spectra on the Brighton to NBS path. Weather clear; high cirrus clouds. Surface temperature < 10°C.

in the observed spectrum. It then becomes a measure of the local power in the spectrum of n in the part of the spectrum sensed by the radar. It is this quantity that we use to compare in-cloud and clear-air scatter to determine whether Bragg scatter is significantly enhanced by clouds. It has been averaged for each event, and it is shown in Table 1.

The strong angular dependence of the Bragg contribution causes it to dominate for small azimuthal deviation (see Fig. 4) even in the presence of appreciable cloud and precipitation, but a few degrees off the baseline the signal approaches the incoherent "floor" and the incoherent term becomes comparable to the Bragg term. In calculating $\phi(\kappa)$ the pure Bragg component was extracted by subtracting the power in the (incoherent) backscatter from the total power measured in forward scatter. For 3 cm wavelength radars, it was considered that the backscatter ($\theta = 180°$) could be safely assumed to be entirely incoherent.

The figures show that the several runs made on any one day are generally very consistent with each other. The variability from day to day is generally much greater as seen in Table 1 and suggests that the variability is real and of natural origin, but it is not clear whether it represents a genuine variability in the refractive index spectrum or horizontal inhomogeneity as the common volume is moved horizontally. Such horizontal movement was typically about a kilometer, and the beamswinging typically lasted about an hour with each swing taking ~10 min. It seems unlikely that consistent inhomogeneity would persist over the same kilometer for as long as an hour.

The days showing the greatest variability between successive beam swingings were 11 April and 9 October 1979. On 11 April the clouds were dense and widespread, and they extended to the surface. The power versus azimuth data from which the spectra of Fig. 10 were plotted are shown in Fig. 4 and the power decrease in the Bragg range is seen to be fairly ragged. The spectra for 11 April (and for 19 March) were plotted (Figs. 9 and 10) using an ordinate that was the difference of $\log\phi(\kappa)$ from its value on the baseline at the minimum scattering angle (solid circle). This was done to reveal more clearly the slope of the spectra when the power from spectrum to spectrum varied substantially. We believe the abnormally large variability on some days is caused by time variability in the large-scale inhomogeneity of the very elongated volume from which forward scatter is received. On days with cloud/precipitation the liquid-water inhomogeneity could be monitored in the backscatter mode. For example, the variability in decibels of reflectivity (dBZ) in backscatter was large on 11 April, even exceeding the variability in decibels of C_n^2. The reflectivity versus sample

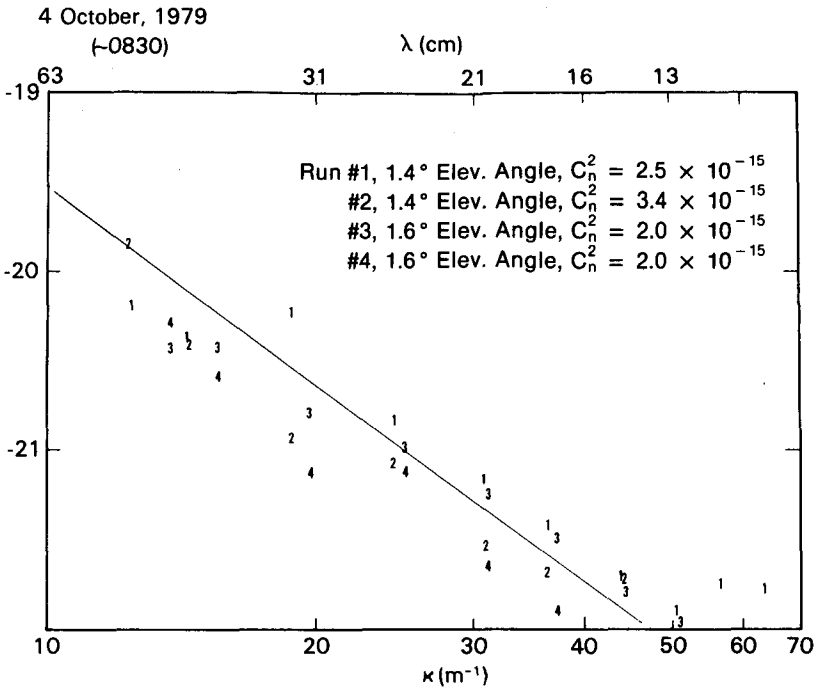

FIG. 12. Scatterer spectra on the Brighton to NBS path. Weather clear. A few cirrus clouds. Surface temperature < 10°C. Pronounced temperature inversion aloft (see Fig. 15).

number is shown in Fig. 14. Each sample consisted of a file of data at successive azimuthal increments out to 2.5 or 3° from the baseline and large steps of ~5° out to 30° off baseline. (A file was recorded at 65° azimuth between runs 1 and 2.) After sample 60 the azimuthal increment near the baseline was changed from 0.5 to 1° to speed up the azimuthal scan. Various off-baseline azimuth

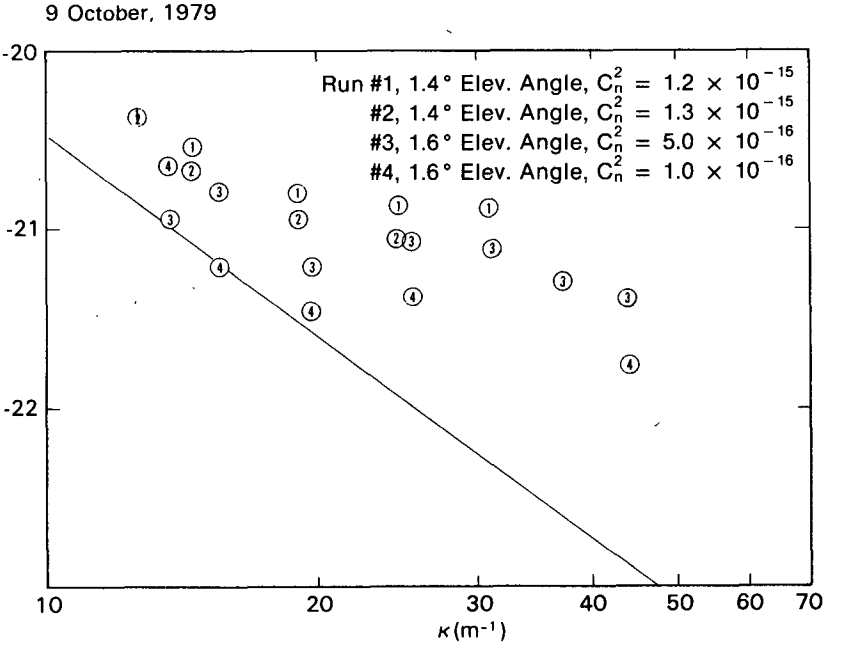

FIG. 13. Scatterer spectra on the Brighton to NBS path. Light rain or drizzle and snow. Cloud base < 300 m AGL when observations began at 1000 MST.

TABLE 1. Summary of results.

Date	$-(m+2)$	$\overline{C_n^2}$	Weather
1/31/79	−4.7	6.5×10^{-16}	Clear
2/15/79	−2.5	2.6×10^{-15}	Cloud
2/27/79	−4.9	4.0×10^{-14}	Clear
3/19/79	−4.2	2.4×10^{-14}	Mixed
4/11/79	−3.43	1.1×10^{-14}	Cloud
10/03/79	−2.46	4.4×10^{-15}	Clear
10/04/79	−3.10	3.7×10^{-15}	Clear
10/09/79	−1.49	1.0×10^{-15}	Cloud/light rain/snow
Average 3.7 clear			
Average 2.9 cloud			

angles at which Z was measured are indicated on the figure. Near the baseline azimuth (0°) the values of C_n^2 from forward scatter were (in time sequence) 9.3×10^{-15}, 1.7×10^{-14}, 1.2×10^{-14} and 5.7×10^{-15}. There seems to be no significant relation between the strength of the Bragg return and the incoherent scatter. The correlation, if anything, is negative.

We believe that any uncertainty in the conclusions that can be drawn from this experiment does not relate to accuracy or reliability of the observational data, but rather to interpretation, and assumptions about the scattering entities:

1) The necessary assumption of statistical homogeneity in the roughly double-conical scattering volume and the requirement of temporal and horizontal spatial homogeneity over the kilometer of horizontal distance that the beams were swung.

2) The assumption that the scattering comes either from hydrometeors or from the atmospheric gas. Birds and aircraft occasionally passed through the scattering volume or side lobes of the radar antenna patterns causing anomalous scattered power to enter the receivers. These were usually obvious and recording was stopped until normal conditions returned. Such events also were edited out of the data in the post processing when they were obvious. However, some contamination by marginal events undoubtedly remains. Insects are a major contribution to radar return in Colorado in the summer months. In fact, they precluded useful experiments during that season. Insects appeared in the records when surface temperatures exceeded ~10°C and disappeared in the fall after surface temperatures first dropped below 10°C. They were a major factor in our experimental program and were the cause of the long gap in measurements between April and October. They limited our observations to the stratiform, up-slope clouds of winter storms in Colorado. In spite of our efforts to ensure the absence of insects in our scattering volume, there remains some uncertainty as to whether their effects were completely eliminated.

3) The thermal stability (temperature stratification) of the height region encompassing the scattering volume. Fig. 15a–15f shows the temperature

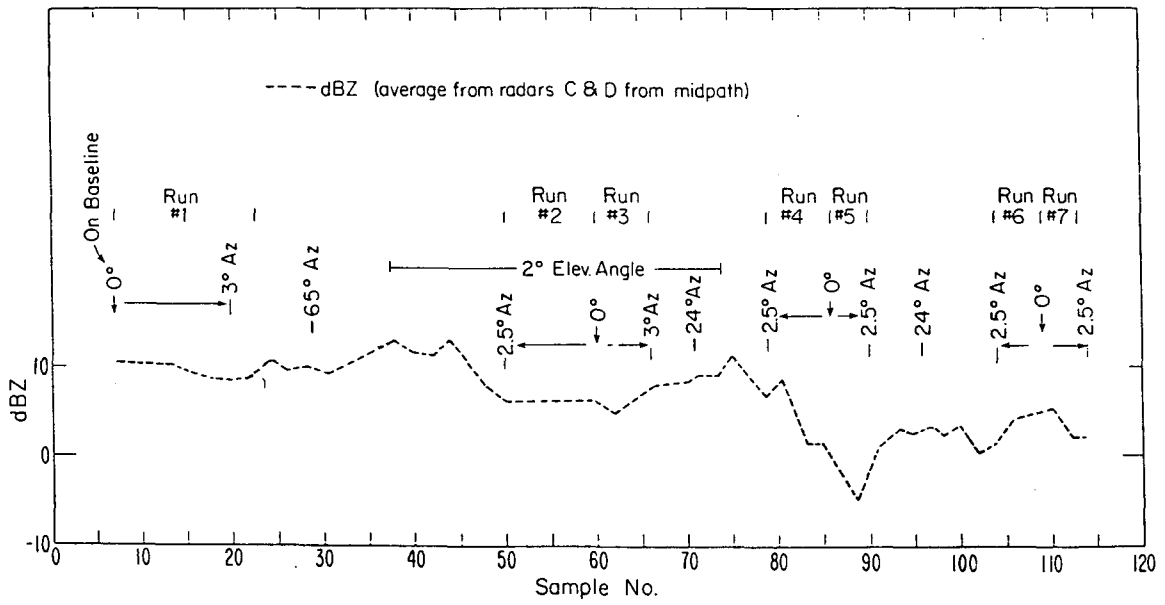

FIG. 14. Observed reflectivity factor (dB) for seven beams swingings on 11 April 1979 for a case when cloud and snow extended down to the surface. Each sample consists of a file of data at half-degree azimuthal increments out to 2.5 or 3° from baseline and large steps of about 5° out to 30° off the baseline (see Fig. 4). A file was recorded at 65° azimuth between Runs 1 and 2. After sample number 60 the azimuthal increment near the baseline was increased from 0.5 to 1.0°. Backscatter was recorded by both radars. The curve is the average of Z computed from the backscatter measured by the two radars after adding 2 dB to the signal measured by the Boulder radar to match calibrations.

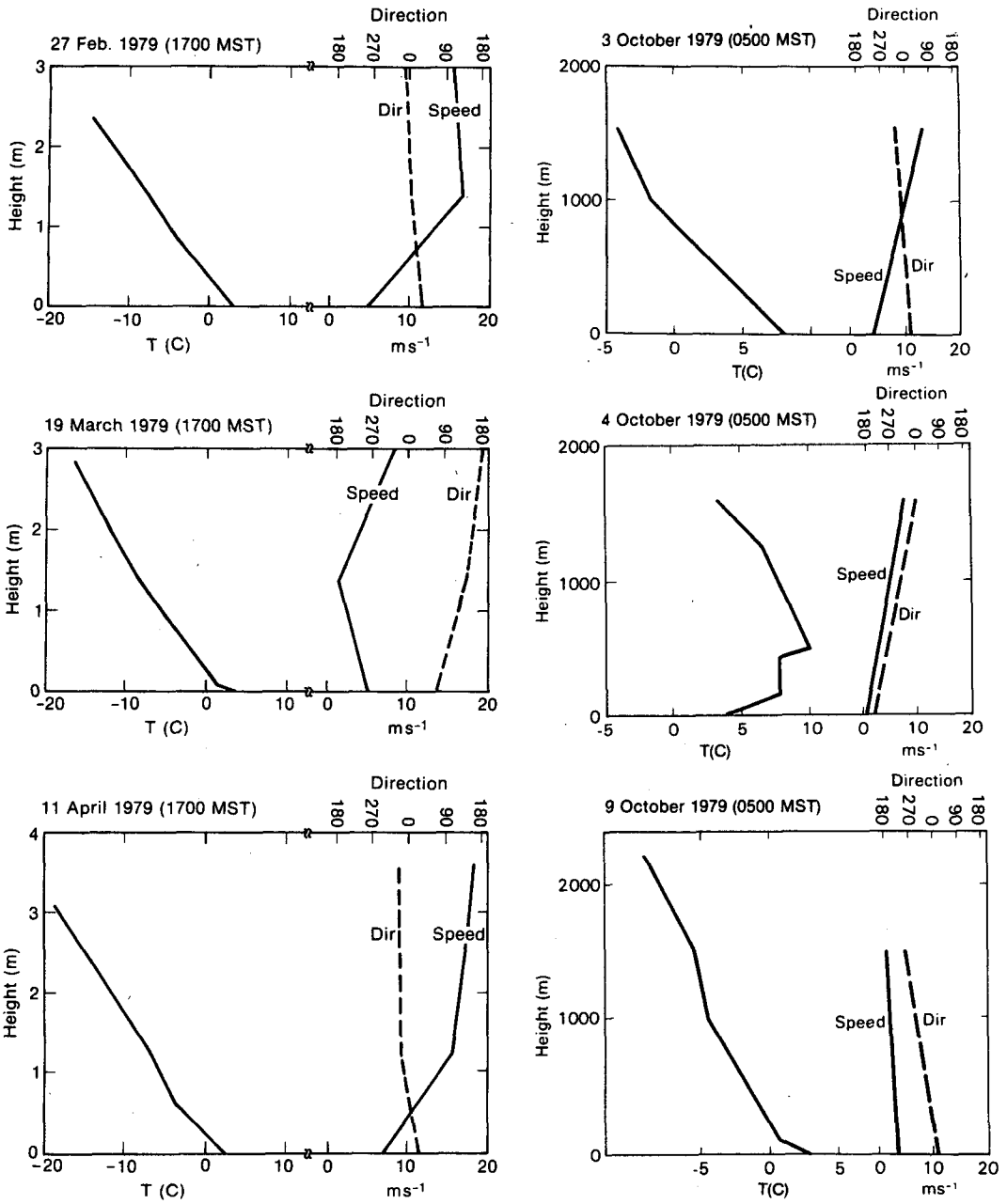

FIG. 15. Rawinsonde data for scattering events on dates shown.

soundings near the time of the radar observations. The temperature structure of the lowest kilometer of the atmosphere is much more stable on 4 October than on the other cases so stability effects might be expected to cause observable differences in the spectra. However, no such difference is evident and Table 1 shows both the spectral slopes and power densities to be very similar. There is some uncertainty in this conclusion because the raob was taken at Denver (~60 km from the radar path) ~3 h after the radar observations. However, it must be remembered that the spectral scales to which our radar experiment was sensitive were 20–50 cm and the anisotropy resulting from thermal stratification could be expected to be slight. On 31 January a pronounced temperature inversion was present also (Fig. 17), but it was so low that the scattering volume was in the unstable region above it.

From the average regression curve for cloudy days a plot of the crossover in dominance of Bragg-coherent backscatter and incoherent back-

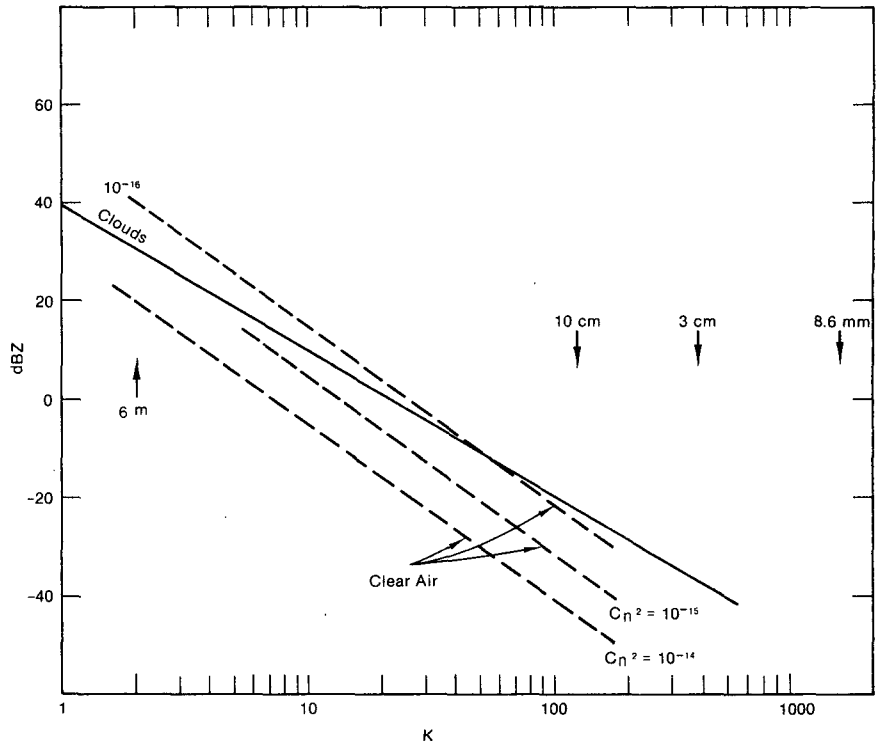

FIG. 16. The dBZ value for transition from Bragg-scatter dominance to incoherent scatter dominance for the typical wavelength range of various radars from regression analysis of all cloud events.

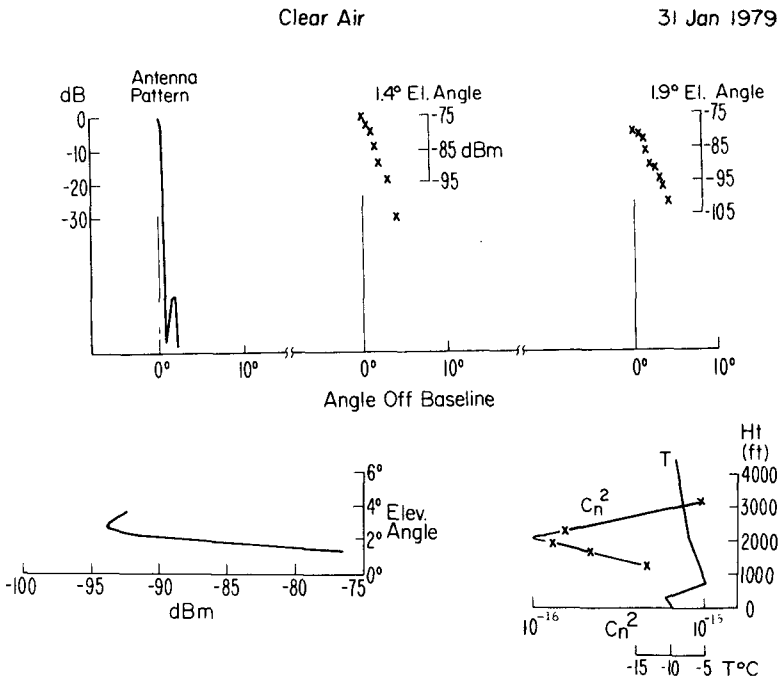

FIG. 17. Clear-air data acquired on 31 January 1979. Both horizontal and vertical beamswinging was done and a height profile of C_n^2 (plotted on a log scale) is shown plotted with the Denver raob temperature from a sounding taken 2 h after the radar observations.

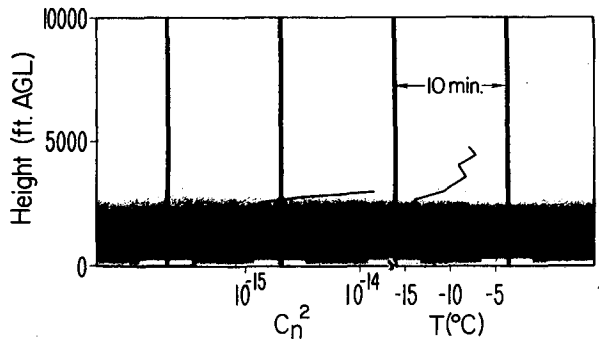

FIG. 18. Height profile of C_n^2 (on log scale) from forward-scatter radar observations on 15 February 1979 superimposed on a facsimile record of cloud backscatter obtained by a vertically pointing 8.6 mm wavelength radar. Temperature sounding is from the Denver raob released ~2 h after radar observations. It shows the frontal inversion capping the cloud layer. The synoptic situation is shown in Fig. 19.

scatter from droplets can be calculated. It is shown in Fig. 16 for our observations which were collected typically in the height interval 500–1000 ms above ground level (AGL) in Colorado. For these observations, Bragg scatter would dominate for a 6 m wavelength radar unless Z exceeded 45 dBZ and would only dominate for Z less than -50 dBZ for an 8.6 mm wavelength radar. For a 3 cm wavelength radar the incoherent return exceeds the Bragg component for all dBZ > -38.

On 31 January and 15 February, forward-scatter scans in the vertical cross section containing the baseline were made from elevation angles of 1.4° (at Boulder) to ~3.5°. For greater elevation angles there was significant blockage by tree limbs. For the case of 31 January, shown in Fig. 17, the weather was clear with fair skies, and the forward scatter was very weak. Lenticular clouds were present over the mountains and the weather was typical of mild local Chinook conditions. Horizontal beam swinging was done at elevation angles of 1.4 and 1.9°. The height profile of C_n^2 is shown on a log scale at the lower right plotted with the temperature sounding from the Denver rawin taken at 1700 MST, 2 h after the radar observations. A prominent low-level subsidence inversion characteristic of this kind of weather condition is evident in the sounding. The radar observations were made above the inversion, since the horizon rays intersected at a height of 1300 ft AGL at midpath. The observed C_n^2 values are understandably very small under these conditions ranging from 10^{-16} to 10^{-15} $m^{-2/3}$.

The results of a vertical beam swinging experiment carried out on 15 February are shown in Fig. 18. The WPL 8.6 mm, vertically pointing radar was also in operation at the time, and its facsimile record is shown as the background of the figure. The 1700 MST temperature sounding from the Denver rawin is also shown on the figure. The height profile of C_n^2 calculated from the forward-scatter radar observations is shown plotted on a log scale. Although there was significant precipitation from the clouds, including some large snowflakes, the cloud layer was obviously very thin and capped by a large temperature inversion. The spectra from the horizontal beam swingings shown in Fig. 8 were from within the cloud layer. Looking at the 1100 MST surface weather map shown in Fig. 19, it is clear that the temperature inversion was a weather front and that the precipitation was related to the local frontal dynamics. Perhaps the most dramatic feature of the forward-scatter data is the very sharp increase (by an order of magnitude) in C_n^2 at the cloud top, which is also the inversion base. This is not altogether unanticipated, since it is to be expected that the entrainment of warm, dry air from above the inversion into the region at the cloud top would produce a locally enhanced variance at that height. Furthermore, this mixing process would lead to a *negative covariance* between temperature and humidity fluctuations which would further enhance the refractive index variance (Gossard, 1960, 1979). On the other hand if in-cloud processes alone are considered, and if the cloud is

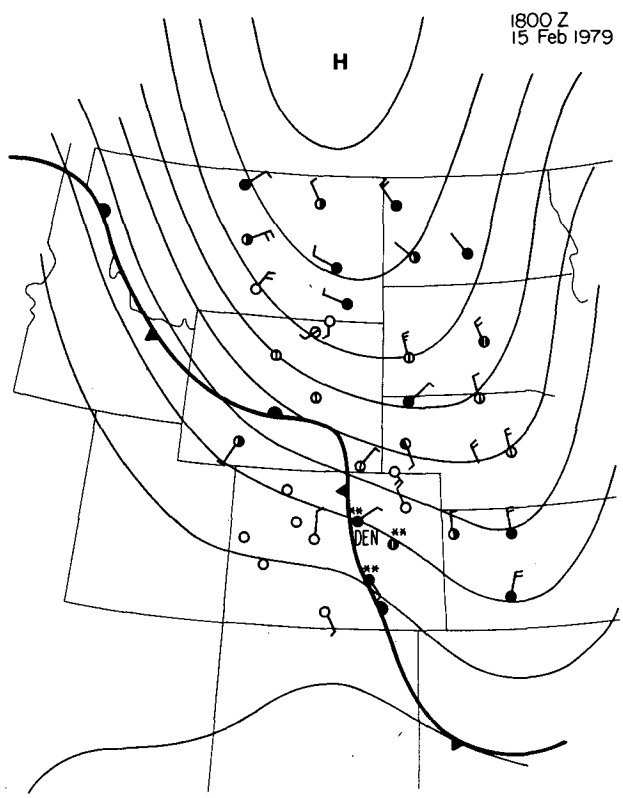

FIG. 19. Surface weather map near the time of the sounding data of Fig. 18.

presumed to be everywhere at or very near saturation, the correlation between temperature and humidity might be presumed to be *positive* because warmer air holds more moisture than colder air (the Clausius-Clapyron relation). This concept of the physics would *diminish* the refractive index variance within the cloud, while the mixing and entrainment occurring at the inversion boundary is likely to produce a pronounced *boundary effect* detectable by vertically pointing radars (Gossard *et al.*, 1978). This boundary effect at interfaces between dry and moist air would exist in the absence of clouds, but in the presence of cloud the effect may be enhanced by the evaporative cooling of penetrating cloud tongues whose evaporation locally increases the humidity increasing the negative covariance.

Other models of in-cloud thermodynamics, such as that of Clark and Hall (1979), can lead to high negative in-cloud covariance between temperature and humidity through supersaturation resulting from finite relaxation time in the evaporation-condensation process. Such models would produce less boundary effect around clouds. Therefore, the techniques used in this paper may provide a useful tool in the study of cloud microphysics.

5. Conclusions

From this study, the following conclusions appear to be justified:

- The forward-scatter radar technique offers an unambiguous way to distinguish incoherent scatter from Bragg scatter.
- Winter clouds/precipitation in the upslope flow conditions of eastern Colorado show no evidence that radar scatter departs significantly from the classical concept of incoherent reflection of radar waves in the wavelength range presently used by meteorological radars. This conclusion may not be valid for summer convective storms.
- There is some evidence of less slope to refractive index spectra inside clouds than would be expected if a $-5/3$ wavenumber dependence were valid.
- Cross-over from dominance of coherent to incoherent backscatter occurs at radar wavelengths of 20–30 cm in those winter cloud/precipitation events observed in this experiment which generally had dBZ values of 0–10.
- There is a dramatic increase in Bragg-coherent return (C_n^2) at cloud tops when they are capped by a temperature inversion with dryer air above. This suggests that negative correlation between temperature and humidity resulting from dry air entrainment into the cloud top may be an important factor in enhanced radar return at cloud boundaries.
- This experiment suggests that the enhanced reflectivities sometimes reported from clouds may be a result of entrainment and mixing of dry air into the cloud rather than thermodynamic enhancement.

REFERENCES

Battan, Louis J., 1973: *Radar Observation of the Atmosphere*. The University of Chicago Press, 324 pp.

Bolgiano, R., 1958: The role of turbulent mixing in scatter propagation. *IRE Trans. Antennas Propag.*, **AP-6,** 161–168.

Booker, H. G., and J. T. DeBettencourt, 1955: Theory of radio transmission by tropospheric scattering using very narrow beams. *Proc. IRE*, **43,** 281–290.

Clark, Terry L., and W. D. Hall, 1979: A numerical experiment on stochastic condensation theory. *J. Atmos. Sci.*, **36,** 470–483.

Gossard, Earl E., 1960: Power spectra of temperature, humidity and refractive index from aircraft and tethered balloon measurements. *IRE Trans. Antennas Propag.*, **AP-8,** 186–201.

——, 1979: A fresh look at the radar reflectivity of clouds. *Radio Sci.*, **14,** 1089–1097.

——, R. B. Chadwick, K. P. Moran, R. G. Strauch, G. E. Morrison and W. C. Campbell, 1978: Observation of winds in the clear air using an FW-CW Doppler radar. *Radio Sci.*, **13,** 285–289.

Kovasnay, L. S. G., M. S. Uberoi and S. Corrsin, 1949: The transformation between one- and three-dimensional power spectra for an isotropic scalar field. *Phys. Rev.*, **76,** 1263–1264.

Ottersten, H., 1969: Radar backscattering from the turbulent clear atmosphere, *Radio Sci.*, **4,** 1251–1255.

Tatarskii, V. I., 1961: *Wave Propagation in a Turbulent Medium*. McGraw-Hill, 285 pp. [Transl. by R. A. Silverman].